Crystal Growth Blocking Strategy Enabling Efficient Solvent-Free Synthesis of Hierarchical UiO-66 for Large-Molecule Catalysis

Jianting Zhang, Jingbo Shi, Hang Zhao, Jinbo Bai, Xiaolin Li, Kunyue Leng

Crystal Growth Blocking Strategy Enabling Efficient Solvent-Free Synthesis of Hierarchical UiO-66 for Large-Molecule Catalysis

Jianting Zhang[1], Jingbo Shi[1], Hang Zhao[1], Jinbo Bai[2], Xiaolin Li[3,], and Kunyue Leng[1,]**

[1] International Collaborative Center on Photoelectric Technology and Nano Functional Materials, Institute of Photonics and Photon-Technology, Northwest University, Xi'an, Shaanxi 710069, China

[2] Université Paris-Saclay, CentraleSupélec, ENS Paris-Saclay, CNRS, LMPS-Laboratoire de Mécanique Paris-Saclay, 8–10 rue Joliot-Curie, 91190 Gif-sur-Yvette, France

[3] Institute of Intelligent Manufacturing Technology Shenzhen Polytechnic, Shenzhen 518055, China

KEY WORDS: MOFs; UiO-66; hierarchical structure; DBT oxidation

ABSTRACT

Metal-organic frameworks (MOFs) with rich hierarchical structure have drawn great attention in the process with large molecule, such as catalysis and adsorption. However, efficiently and cost-effectively fabricating hierarchical MOFs with robust stability remains challenging. Herein, we report a crystal growth blocking strategy to prepare hierarchical UiO-66 by a solvent-free method. The addition of $FeCl_3$ in the synthetic system blocks the overgrowth of UiO-66 crystal and limits the particle size to around just 12 nm. After the removal of Fe by ethanol treatment, these small particles loosely aggregate and gain intercrystalline mesopores. The optimal sample Mes-UiO-66 exhibits well-developed hierarchical structure, the BET surface area reaches 1161.9 m^2g^{-1}, and the mesopore volume attains a state-of-art 1.21 cm^3g^{-1}. The superior catalytic performance and the robust stability of Mes-UiO-66 are demonstrated by the oxidation of DBT, of which the DBT conversion surpasses 99% and shows slight decrease after five cycles. Our finding may provide a novel platform for efficiently fabricating hierarchical MOFs for large molecule catalysis.

INTRODUCTION

Metal-organic frameworks (MOFs), as a well-developed class of porous materials, have drawn much attention in gas adsorption, catalysis and pharmaceutical science, due to the characteristics of large specific surface area and tunable framework structures [1-4]. However, the pore size of most reported MOFs can only be adjusted with micropore regime. The limited accessibility and mass transformation greatly hinder their application when dealing with large guests, such as macromolecule catalysis/ adsorption or large particle capturing [5-8]. Thus, the pivotal obstacle in expanding the application of MOFs with large guests has been focused on enlarging the pore size and the corresponding pore volume, but remains challenging.

Pioneering efforts have been practiced to fabricate MOFs with relatively large pore sizes. Considering the ligand of MOFs is more flexible in size compared with the metal center, the splendid idea of exploiting large organic molecules as ligands has drawn a lots of attention and has been demonstrated successfully [9-11]. However, the complex molecular structures of these ligands greatly increase the preparation cost and cause the problem of poor stability in thermal and chemical solvent environments. In contrast, hierarchical MOFs gained by introducing secondary pore structure in micropore MOFs are more cost-effective and robust. "Top-down" and "bottom-up" are two common strategies to develop hierarchical MOFs from the micropore ones. The “top-down” process employs post-treatment, such as solvent/ acid etching and linker exchange, to excavate caves and holes on MOFs crystals. Despite its simplicity and efficiency, the partial corrosion of the well-crystalized can still negatively affect the stability of MOFs. On the other hand, the "bottom-up" strategy prefers to introduce abundant secondary pores into or between the MOFs crystals during the synthetic process. The ideal hierarchical structure is

commonly obtained by rationally using templates, exquisitely choosing modulators or precisely tuned synthetic conditions [12-14]. For instance, exploiting surfactants (CTAB) as sacrificial templates could create considerable mesoporous in various MOFs [15,16], introducing fatty acids with different chain lengths as regulator provides a splendid platform to regulate the mesoporous [17,18], moreover employing unique synthetic condition such as nano-fusion or supercritical fluid can even fabricate hierarchical MOFs without any additive [13]. Because of the slight impact on the metal-organic frameworks, the original structure is largely preserved under the "bottom-up" strategy, but the insufficient synthesis efficiency and high synthesis costs are still challenging. Together, although remarkable development has been gained, the search for a novel strategy to efficiently fabricate robust hierarchical MOFs with easy-operated process and low-cost is still desired.

UiO-66, made of zirconium base metal nodes and 1,4-dicarboxybenzene (H_2BDC), is one of the most used MOFs. Its excellent stability has been confirmed in water, acidic/ alkaline solutions, most organic solvents and thermal condition up to 500 ^{o}C [19]. Moreover, the original micropore structure of UiO-66 can be developed into hierarchical structure by rationally designed “bottom-up” strategy, although with relatively poor crystalline and low efficiency [20, 21]. Recently, well-crystalized MOFs including UiO-66, can be synthesized efficiently by solvent-free method, which inspired our design of fast fabricating hierarchical UiO-66 with robust stability by modified solvent-free approach [22-25]. Herein, we report a crystal growth blocking strategy for efficiently solvent-free synthesis of hierarchical UiO-66. The addition of Fe salt in solvent-free system successfully limits the crystal size of UiO-66 to between 12 ±2 nm, but leaves slight Fe residue. Moreover, the aggregation of these nano-crystals introduces abundant secondary mesopores to gain well-crystalized hierarchical UiO-66. The optimal sample Mes-

UiO-66 exhibits a remarkable mesopore volume of 1.21cm^3g^{-1}, which is one of the largest in UiO-66. The oxidative desulfurization evaluation demonstrates the superior catalytic ability of Mes-UiO-66 when dealing with large molecules, such as DBT. This work may open up a novel strategy for preparing robust MOFs with rich hierarchical structures.

RESULTS AND DISCUSSION

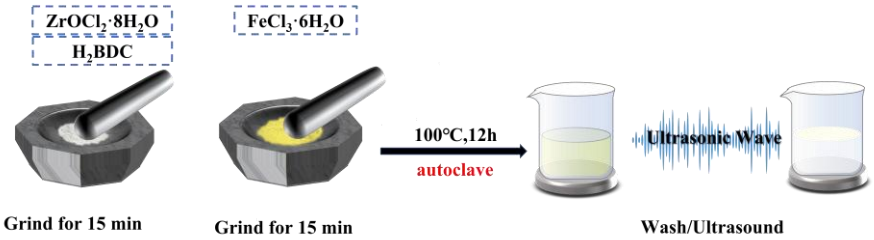

Figure 1. Schematic diagram for the preparation of Mes-UiO-66.

Figure 1 illustrates the synthetic process of the hierarchical UiO-66. Firstly, $ZrOCl_2$•$8H_2O$ and H_2BDC are mixed and ground for 15 min. Then $FeCl_3$•$6H_2O$ is added into the mixture and ground for another 15 min. After crystallizing in an autoclave, the obtained powder is washed by ethanol to remove Fe salt. After drying in vacuum, powder-like hierarchical UiO-66 is gained, which is labeled as Mes-UiO-66. For comparison, samples synthesized without the addition of Fe (UiO-66-solvent free) and synthesized by traditional hydrothermal method (UiO-66-solvent) are also obtained [22]. The effect of the synthetic condition on Mes-UiO-66 is also investigated, including the molar ratio of Fe and Zr ($R_{Fe/Zr}$), crystallization time and crystallization temperature. Based on the evaluation of the crystallinity, BET surface area and mesopore volume, the optimal synthetic condition is indicated as crystalizing at 100 ^oC for 12 h with a $R_{Fe/Zr}$ of 3.（Figure S1-3, Table S1-3）

Figure 2a shows the XRD patterns of various UiO-66. In agreement with UiO-66-solvent and UiO-66-solvent free, Mes-UiO-66 displays well-resolved diffraction peaks of UiO-66 structure at 7.4 and 8.5 degree, and no peaks of any crystal impurity are observed. The broader peak width of Mes-UiO-66 compared with that of UiO-66-solvent imply its relatively small particle size. The results of XRD suggest that the addition of Fe salt is incapable of impacting the crystallization process or inducing the nucleation of any undesired crystal, agreed with the well thermal stability of Mes-UiO-66 before and after activation (Figure 2b and Figure S4). Moreover, the ICP and XPS results confirmed the negligible residue of Fe in Mes-UiO-66, (Table S4 and Figure S5), demonstrating the Fe salt is more favorable to act as mesoporous-inducing agent than to combine into the framework of Mes-UiO-66.

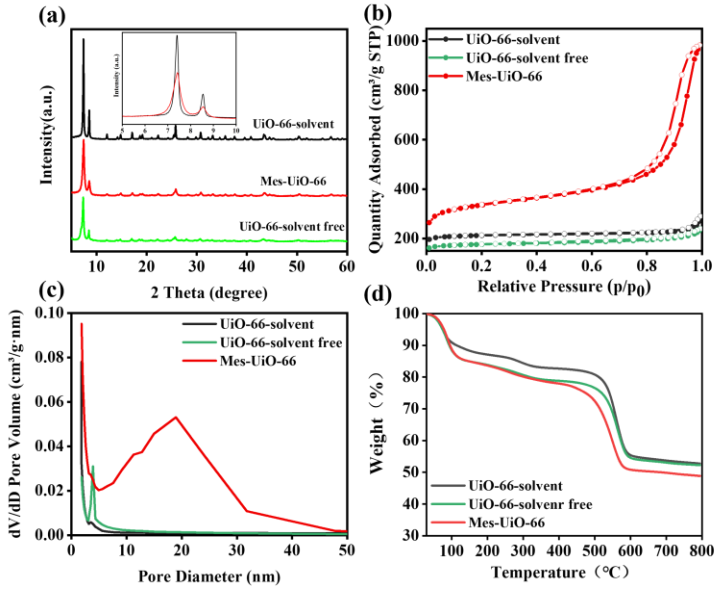

Figure 2. (a) XRD patterns, (b) TG curves, (c) N_2 sorption isotherms and (d) pore size distribution of UiO-66-solvent, UiO-66-solvent free and Mes-UiO-66.

The hierarchical structure of Mes-UiO-66 is firstly investigated by N_2 adsorption-desorption test, and the N_2 sorption isotherms are shown in Figure 2c. UiO-66-solvent and UiO-66-solvent

free exhibit the typical type I isotherms, indicating the predominant micropore structure in the two samples. In comparison, Mes-UiO-66 displays type I and IV isotherm with a hysteresis loop, demonstrating the existence of both micropore and mesopore structure, which solid defined the hierarchical structure of Mes-UiO-66. The detailed N_2 sorption results are listed in Table 1. Mes-UiO-66 displays a BET surface area of 1161.9 m^2g^{-1}, slightly higher than that of UiO-66-solvent and UiO-66-solvent free. Interestingly, the mesopore volume of Mes-UiO-66 reaches 1.21 cm^3g^{-1}, over five times as that of UiO-66-solvent (0.21 cm^3g^{-1}) and UiO-66-solvent free (0.24 cm^3g^{-1}). Moreover, the affluent mesopore structure of Mes-UiO-66 surpasses most of the reported hierarchical UiO-66 (Table S5). The pore distributions are calculated based on the BJH desorption branch. As shown in Figure 2d, in agreement with the isotherms, UiO-66-solvent and UiO-66-solvent free exhibit almost no pores between 2-50 nm (the peaks around 4 nm are caused by the instrumental error), confirming the absence of mesopore. But for Mes-UiO-66, a peak centers around 18 nm is observed between the range of 5 to 32 nm. Considering the good crystallinity of Mes-UiO-66, the relatively broad mesopore distribution may be the result of the accumulation of small crystal.

Table 1. Detailed N_2 sorption results of various samples.

Sample	S_{BET} (m^2g^{-1}) [a]	V_{total} (cm^3g^{-1}) [b]	V_{micro} (cm^3g^{-1}) [a]	V_{meso} (cm^3g^{-1}) [c]	$S_{external}$ (m^2g^{-1}) [a]
Mes-UiO-66	1161.9	1.51	0.30	1.21	412.4
UiO-66-solvent free	1078.0	0.65	0.41	0.24	114.9
UiO-66-solvent	798.0	0.50	0.31	0.21	87.6

[a] t-plot method

[b] desorption total pore volume

[c] BJH desorption branch

To further reveal the origin of the hierarchical structure, the morphology of UiO-66 synthesized by different methods is investigated. The SEM images of Mes-UiO-66, UiO-66-solvent and UiO-66-solvent-free all disclose the unordered aggregation of particles, but the size and the packing degree of different MOFs are discrepant (Figure S6-8). As shown in Figure 3, the TEM images confirmed that the average diameter of Mes-UiO-66 is around12±2 nm, much smaller than that of UiO-66-solvent (105±20 nm) and UiO-66-solvent-free (65±10 nm), in good agreement with the broader diffraction peaks of Mes-UiO-66. Moreover, Mes-UiO-66 displays a relatively loose aggregation of the small particles, in which abundant interstices and spaces can be obviously observed (Figure 3c-d and Figure S9). In contrary, the particles of UiO-66-solvent and UiO-66-solvent-free clung tightly, leaving just a little space between each particle. Thus, it can be demonstrated that the abundantly hierarchical structure in Mes-UiO-66 stem from the nano-scale crystal and their unconsolidated accumulation, which should be attributed to the addition of Fe salt during the synthetic process.

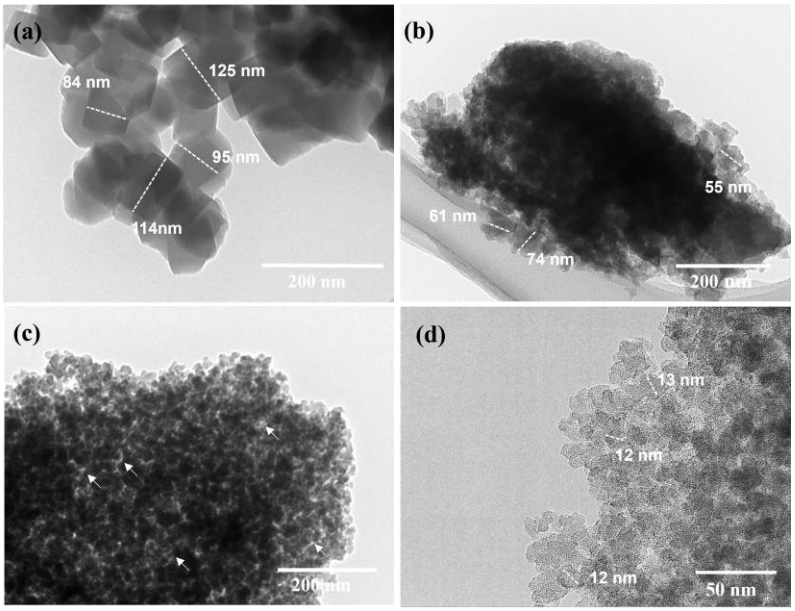

Figure 3. TEM images of (a) UiO-66-solvent, (b) UiO-66-solvent free, (c, d) Mes-UiO-66.

In order to clarify the role of $FeCl_3$ in the formation of hierarchical structure in Mes-UiO-66, other chloride salts, such as NaCl, KCl, $CuCl_2$ and $CoCl_2$, are employed as substitute of $FeCl_3$ to prepare UiO-66. As shown in Figure 4a, the addition of $CuCl_2$ and $CoCl_2$ results in quite weak diffraction peaks of UiO-66. Although the samples synthesized with the addition of NaCl and KCl show well-resolved diffraction peak of UiO-66, but the low BET surface area and mesopore volume reveal the insufficient secondary pore structure (Figure 4b and Table S6). Moreover, $FeCl_2$ and $Fe(NO_3)_3$ are also used as additive to synthesize hierarchical UiO-66, but fail to gain crystalline UiO-66. Moreover, it can be indicated that the $FeCl_3$ does not just act as a salt template for mesopores, despite it is can be totally removed by ethanol washing after the synthetic process. The $FeCl_3$ should participate the crystal growth of UiO-66 and block it from growing big. The above results reveal the uniqueness of $FeCl_3$ in inducing hierarchical structure in the solvent-free synthesis of UiO-66， which may benefit from the easy interaction and dissociation of $FeCl_3$ with UiO-66 framework.

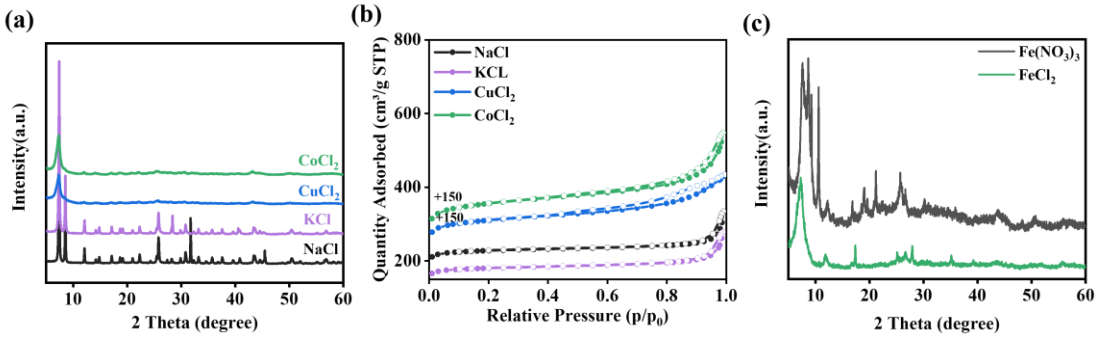

Figure 4. (a) XRD patterns and (b) N_2 sorption isotherms of UiO-66 prepared with the addition of $CoCl_2$, $CuCl_2$, KCl and NaCl, (c) XRD patterns of samples prepared with the addition of Fe_2Cl and $Fe(NO_3)_3$.

The impaction of the interaction of Zr center and the H_2BDC (linker) caused by the addition of hetero metal salts should contribute to the small particle size of Mes-UiO-66. Thus, we first practice the acid-base titration to investigate the effect of the $FeCl_3$ on the missing linker. Figure 5a-c show the acid-base titration curves and the corresponding first derivative curves. The acid-base titration curve of UiO-66-solvent illustrates three inflection points (Figure 5a), which belong to the μ_3-OH proton stem from the framework of UiO-66, Zr-OH_2 proton and Zr-OH proton caused by the missing linker, respectively. The UiO-66-solvent free shows similar inflection points (Figure 5b). Interestingly, the Mes-UiO-66 only displays the inflection of μ_3-OH proton, the inflections of Zr-OH_2 proton and Zr-OH proton are hard to be detected (Figure 5c). Based on the first derivative curve, the number of missing linkers in Mes-UiO-66 is calculated to 0.125, much smaller than in UiO-66-solvent (1.625) and in UiO-66-solvent-free (2.155, Table S7-9). The results of the acid-base titration demonstrate that the $FeCl_3$ has slight impaction on the initial combination of H_2BDC into Mes-UiO-66 to form small crystal. To reveal the impaction of $FeCl_3$ on the Zr center, Zr 3d XPS is characterized over Mes-UiO-66 before and after ethanol washing. As shown in Figure 5d, the Zr $3d_{5/2}$ binding energy of the sample without ethanol washing (just synthesized Mes-UiO-66) is confirmed as 183.2 eV, in good agreement with the reported Zr(IV)-O-Fe(III) coordination in UiO-66, indicating the temporary connection of Fe on the surface of Mes-UiO-66 particles by O bridge [26]. However, after the ultrasonic treatment in ethanol, the Zr $3d_{5/2}$ binding energy of Mes-UiO-66 negatively shifting to 182.8 eV, suggesting the removal of the Fe. The stripping of the connecting Fe from Mes-UiO-66 can also be confirmed by the color change of Mes-UiO-66 from yellow to white, the bright yellow appearance of the used ethanol and the absence of the Fe-O vibration around 520 cm^{-1} in FT-IR spectra (Figure 5e and Figure S10) [27-29]. Moreover, the Mes-UiO-66 still

exhibits higher oxidative state even after ethanol washing (Figure 5f), which results in the higher zeta potential of Mes-UiO-66 in ethanol (38 mV) compared with that of UiO-66-solvent (14 mV) and UiO-66-solvent-free (22 mV, Figure 5g-i), demonstrating the increasing positive charge on the surface of Mes-UiO-66. Therefore, the forming pathway of the hierarchical Mes-UiO-66 can be disclosed. Firstly, Zr species react with H_2BDC to form small UiO-66 particles. Then, the Fe species connect with the Zr at the surface of particles, which blocks the further growth of these small particles with H_2BDC. Finally, after the removal of Fe by ethanol washing, the relatively high surface positive charge enables loose aggregation of these particles, which lead to the abundant hierarchical structure.

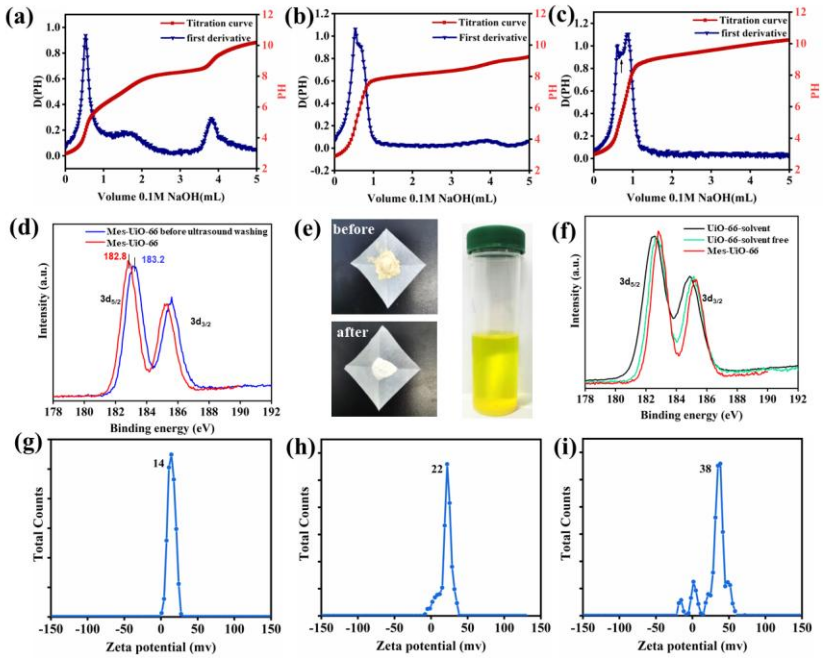

Figure 5. Acid-base titration curve and first derivative curve of (a) UiO-66-solvent, (b) UiO-66-solvent free and (c) Mes-UiO-66. (d) Zr 3d XPS of the just synthesized and ethanol washed Mes-UiO-66. (e) Digital images of the as synthesized and ethanol washed Mes-UiO-66 and the used ethanol. (f) Zr 3d XPS spectra of various samples. Zeta potential of (g) UiO-66-solvent, (h) UiO-66-solvent free and (i) Mes-UiO-66 in ethanol.

The oxidizing Zr center, abundant hierarchical structure and rich surface positive charge of Mes-UiO-66 provide an ideal platform for the catalytic oxidation of aromatic large molecules. Thus, the oxidation of dibenzothiophene (DBT) with tert-butyl hydroperoxide (TBHP) at 60 ^{o}C is firstly employed to evaluate the catalytic performance of Mes-UiO-66. As shown in Figure 6a, only 14% of DBT can be oxidized when UiO-66-solvent is used as catalyst. The UiO-66-solvent free displays a DBT conversion of 38% after 4 h. The Mes-UiO-66 shows the best ability to trigger the oxidation of DBT. After 4 hours almost all the DBT is removed by TBHP (DBT conversion surpasses 99%). Moreover, the DBT conversion over Mes-UiO-66 just shows slight decrease after five cycles (Figure 6b), indicating its robust stability. The superior catalytic performance of Mes-UIiO-66 can be attributed to its hierarchical structure that reduces the mass transfer limitation and the rich surface positive that enhances the interaction with aromatic molecule. Furthermore, the superior catalytic performance of Mes-UiO-66 is also confirmed in the oxidation of cyclohexene (Figure S11).

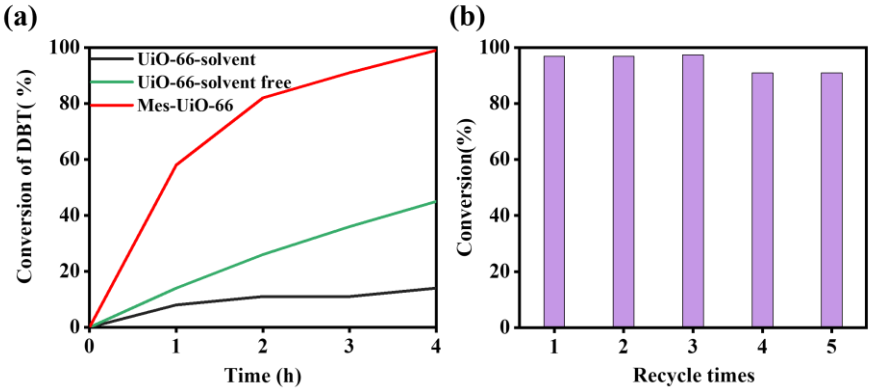

Figure 6. (a) DBT conversion over Mes-UiO-66, UiO-66-solvent and UiO-66-solvent-free. (b) stability tests of Mes-UiO-66.

CONCLUSION

In conclusion, we report a simple and efficient method for synthetic hierarchical UiO-66, by grinding $ZrOCl_2 \cdot 8H_2O$, H_2BDC with $FeCl_3 \cdot 6H_2O$ and crystalizing at 100 ^oC without solvent. The addition of $FeCl_3$ successfully limits the crystal size of UiO-66 to around 12 ± 2nm. After the totally removing of Fe by ethanol washing, the loose aggregation of these small particles leads to rich intercrystalline mesopores. The resultant hierarchical sample Mes-UiO-66 exhibits a BET surface area of 1161.9 m^2g^{-1} and a state-of-art mesopore volume of 1.21 cm^3g^{-1}. The abundant hierarchical structure of Mes-UiO-66 enables superior catalytic performance in the oxidation of DBT. The DBT conversion surpasses 99% after 4 h. Our finding may provide a novel platform to efficiently fabricating hierarchical MOFs for large molecule catalysis.

EXPERIMENTAL SECTION

Synthetic method

Mes-UiO-66: $ZrOCl_2 \cdot 8H_2O$(1.8mmol) and H_2BDC(1.8mmol) were mixed at room temperature, manually ground in mortar for about 15 min, and then $FeCl_3 \cdot 6H_2O$ was added in a certain proportion for further grinding for 15 min. The obtained material was transferred to an autoclave and crystallized at a certain temperature and time. After cooling to room temperature, the resulting solid was washed with ethanol at 60 ℃ and sonicated for 90 min, followed by vacuum drying at 80 °C for 12 h.

UiO-66-solvent: UiO-66-solvent was prepared by the method reported [19]. The detailed steps are shown in the Supporting Information.

UiO-66-solvent free: UiO-66-solvent mainly refer to the reported method [22]. The detailed steps are shown in the Supporting Information.

ASSOCIATED CONTENT

Supporting Information

The online version of this article (http://dx.doi.org/10.1007/s12274-***-****-*) contains supplementary material, which is available to authorized users.

AUTHOR INFORMATION

*Corresponding Author

Kunyue Leng − International Collaborative Center on Photoelectric Technology and Nano Functional Materials, Institute of Photonics and Photon-Technology, Northwest University, Xi'an, Shaanxi 710069, China; Email: lengky@nwu.edu.cn (K.L.)

Xiaolin Li− Institute of Intelligent Manufacturing Technology Shenzhen Polytechnic, Shenzhen 518055, China; Email: lixiaolin0427@szpt.edu.cn (X.L.)

Author Contributions

The manuscript was written through contributions of all authors. All authors have approved the final version of the manuscript.

Notes

The authors declare no conflict of interest.

ACKNOWLEDGEMENTS

This work was financially supported by the National Natural Science Foundation of China (51873174, and 52105307), Natural Science Foundation of Shaanxi Province (2022JQ082 and 2022JM286), Guangdong Basic and Applied Basic Research Foundation (2021A1515011808), Shenzhen Science and Technology Program (RCBS20210609104444087), Research Funding of Post-doctoral Who Came to Shenzhen (4103-6021271018K1), Scientific Research Start-up Project of Shenzhen Polytechnic (4103-6022312030K).

REFERENCES

1. Ryu, U.; Jee, S.; Rao, P. C.; Shin, J.; Ko, C.; Yoon, M.; Park, K. S.; Choi, K. M., Recent advances in process engineering and upcoming applications of metal-organic frameworks. *Coord Chem Rev* **2021,** *426*, 213544.

2. Khan, N. A.; Hasan, Z.; Jhung, S. H., Beyond pristine metal-organic frameworks: Preparation and application of nanostructured, nanosized, and analogous MOFs. *Coord Chem Rev* **2018,** *376*, 20-45.

3. Xiang, W.; Zhang, Y.; Chen, Y.; Liu, C.-j.; Tu, X., Synthesis, characterization and application of defective metal–organic frameworks: current status and perspectives. *J. Mater. Chem. A* **2020,** *8* (41), 21526-21546.

4. Feng, L.; Wang, K. Y.; Lv, X. L.; Yan, T. H.; Zhou, H. C., Hierarchically porous metal-organic frameworks: synthetic strategies and applications. *Natl Sci Rev* **2020,** *7* (11), 1743-1758.

5. Wen, T.; Quan, G.; Niu, B.; Zhou, Y.; Zhao, Y.; Lu, C.; Pan, X.; Wu, C., Versatile Nanoscale Metal-Organic Frameworks (nMOFs): An Emerging 3D Nanoplatform for Drug Delivery and Therapeutic Applications. *Small* **2021,** *17* (8), e2005064.

6. Bavykina, A.; Kolobov, N.; Khan, I. S.; Bau, J. A.; Ramirez, A.; Gascon, J., Metal-Organic Frameworks in Heterogeneous Catalysis: Recent Progress, New Trends, and Future Perspectives. *Chem Rev* **2020,** *120* (16), 8468-8535.

7. Duan, C.; Li, F.; Yang, M.; Zhang, H.; Wu, Y.; Xi, H., Rapid Synthesis of Hierarchically Structured Multifunctional Metal–Organic Zeolites with Enhanced Volatile Organic Compounds Adsorption Capacity. *Ind. Eng. Chem. Res.* **2018,** 57, 15385–15394.

8. Shen, K.; Zhang, L.; Chen, X.; Liu, L.; Zhang, D.; Han, Y.; Chen, J.; Long, J.; Luque, R.; Li, Y.; Chen, B., Ordered macro-microporous metal-organic framework single crystals. *Science* **2018,** *359* (6372), 206-210.

9. Cirujano, F. G.; Martin, N.; Wee, L. H., Design of Hierarchical Architectures in Metal–Oganic Frameworks for Catalysis and Adsorption. *Chem. Mater.* **2020,** *32* (24), 10268-10295.

10. Zhang, X.; Tu, R.; Lu, Z.; Peng, J.; Hou, C.; Wang, Z., Hierarchical mesoporous metal–organic frameworks encapsulated enzymes: Progress and perspective. *Coord Chem Rev* **2021,** *443,* 214032.

11. Feng, D.; Liu, T. F.; Su, J.; Bosch, M.; Wei, Z.; Wan, W.; Yuan, D.; Chen, Y. P.; Wang, X.; Wang, K.; Lian, X.; Gu, Z. Y.; Park, J.; Zou, X.; Zhou, H. C., Stable metal-organic

297 frameworks containing single-molecule traps for enzyme encapsulation. *Nat Commun* **2015,**
298 *6*, 5979.

299 12. Li, K.; Yang, J.; Gu, J., Hierarchically Porous MOFs Synthesized by Soft-Template
300 Strategies. *Acc Chem Res* **2022,** *55* (16), 2235-2247.

301 13. Peng, L.; Zhang, J.; Xue, Z.; Han, B.; Sang, X.; Liu, C.; Yang, G., Highly mesoporous
302 metal-organic framework assembled in a switchable solvent. *Nat Commun* **2014,** *5*, 4465.

303 14. Cai, G.; Jiang, H. L., A Modulator-Induced Defect-Formation Strategy to Hierarchically
304 Porous Metal-Organic Frameworks with High Stability. *Angew Chem Int Ed Engl* **2017,** *56*
305 (2), 563-567.

306 15. Wang, S.; Wang, T.; Zheng, H.; Fan, F.; Gu, Z.; He, W.; Zhang, B.; Shao, L.; Chen, H.;
307 Li, Y.; Zhang, X.; Zhang, L.; Fu, Y.; Qi, W., Fabrication of mesoporous MOF nanosheets
308 via surfactant-template method for C–S coupling reactions. *Micropor. Mesopor. Mat.* **2020,**
309 *303,* 110254.

310 16. Molina, M. A.; Habib, N. R.; Díaz, I.; Sánchez-Sánchez, M., Surfactant-induced
311 hierarchically porous MOF-based catalysts prepared under sustainable conditions and their
312 ability to remove bisphenol A from aqueous solutions. *Catal. Today* **2022,** *394-396*, 117-124.

313 17. Ardila-Suarez, C.; Molina, V. D.; Alem, H.; Baldovino-Medrano, V. G.; Ramirez-
314 Caballero, G. E., Synthesis of ordered microporous/macroporous MOF-808 through
315 modulator-induced defect-formation, and surfactant self-assembly strategies. *Phys Chem*
316 *Chem Phys* **2020,** *22* (22), 12591-12604.

18. Zhao, T.; Li, S.; Xiao, Y.-X.; Janiak, C.; Chang, G.; Tian, G.; Yang, X.-Y., Template-free synthesis to micro-meso-macroporous hierarchy in nanostructured MIL-101(Cr) with enhanced catalytic activity. *Sci. China Mater.* **2020,** *64* (1), 252-258.

19. Cavka, J. H.; Jakobsen, S.; Olsbye, U.; Guillou, N.; Lamberti, C.; Bordiga, S.; Lillerud, K. P., A new zirconium inorganic building brick forming metal organic frameworks with exceptional stability. *J. Am. Chem. Soc.* **2008,** *130* (42), 13850-13851.

20. Feng, L.; Yuan, S.; Zhang, L. L.; Tan, K.; Li, J. L.; Kirchon, A.; Liu, L. M.; Zhang, P.; Han, Y.; Chabal, Y. J.; Zhou, H. C., Creating Hierarchical Pores by Controlled Linker Thermolysis in Multivariate Metal-Organic Frameworks. *J. Am. Chem. Soc.* **2018,** *140* (6), 2363-2372.

21. Hao, L.; Li, X.; Hurlock, M. J.; Tu, X.; Zhang, Q., Hierarchically porous UiO-66: facile synthesis, characterization and application. *Chem Commun (Camb)* **2018,** *54* (83), 11817-11820.

22. Ye, G.; Zhang, D.; Li, X.; Leng, K.; Zhang, W.; Ma, J.; Sun, Y.; Xu, W.; Ma, S., Boosting Catalytic Performance of Metal-Organic Framework by Increasing the Defects via a Facile and Green Approach. *ACS Appl Mater Interfaces* **2017,** *9* (40), 34937-34943.

23. Friščić, T., New opportunities for materials synthesis using mechanochemistry. *J. Mater. Chem.* **2010,** *20,* 7599-7605.

24. Fu, J.; Wu, Y. N., A Showcase of Green Chemistry: Sustainable Synthetic Approach of Zirconium-Based MOF Materials. *Chem. Eur. J.* **2021,** *27*, 9967-9987.

25. Uzarevic, K.; Wang, T. C.; Moon, S. Y.; Fidelli, A. M.; Hupp, J. T.; Farha, O. K.; Friscic, T., Mechanochemical and solvent-free assembly of zirconium-based metal-organic frameworks. *Chem Commun (Camb)* **2016,** *52* (10), 2133-2136.

26. Xu, C. Y.; Pan, Y. T.; Wan, G.; Liu, H.; Wang, L.; Zhou, H.; Yu, S. H.; Jiang, H. L., Turning on Visible-Light Photocatalytic C-H Oxidation over Metal-Organic Frameworks by Introducing Metal-to-Cluster Charge Transfer. *J. Am. Chem. Soc.* **2019,** *141* (48), 19110-19117.

27. Lin, Y. X.; Zhang, Y.; Li, G. J., Promotion of sulfameter degradation by coupling persulfate and photocatalytic advanced oxidation processes with Fe-doped MOFs. *Sep. Purif. Technol.* **2022,** *282*, 119632.

28. Jiang, S.; Zhang, Y.; Wang, S.; Chen, Z.; Yu, L.; Wang, M.; Zhang, X.; Lyu, Y.; Feng, J.; Li, M.; Xiong, W., Novel core-shell Fe-UiO-66/silicalite-1 catalysts for efficient degradation of phenolic wastewater. *J. Environ. Chem. Eng.* **2021,** *9* (6), 106840.

29. Hu, P.; Liang, X.; Yaseen, M.; Sun, X.; Tong, Z.; Zhao, Z.; Zhao, Z., Preparation of highly-hydrophobic novel N-coordinated UiO-66(Zr) with dopamine via fast mechano-chemical method for (CHO-/Cl-)-VOCs competitive adsorption in humid environment. *Chem. Eng. J.* **2018,** *332*, 608-618.

For Table of Contents Use Only

Crystal Growth Blocking Strategy Enabling Efficient Solvent-Free Synthesis of Hierarchical UiO-66 for Large-Molecule Catalysis

*Jianting Zhang[1], Jingbo Shi[1], Hang Zhao[1], Jinbo Bai[2], Xiaolin Li[3], * and Kunyue Leng[1], **

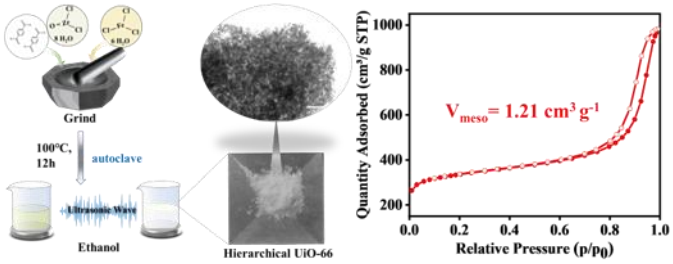

we report a crystal growth blocking strategy for efficiently solvent-free synthesis of hierarchical UiO-66. The addition of Fe salt in solvent-free system successfully limits the crystal size of UiO-66 to between 12 ±2 nm, the loose aggregation of these nanocrystals introduced abundant intercrystalline mesopores to obtain well-crystallized stratified UiO-66. The resultant Mes-UiO-66 exhibits well-developed hierarchical structure, the BET surface area reaches 1161.9 m^2g^{-1}, and the mesopore volume attains a state-of-art 1.21 cm^3g^{-1}.